INTERNATIONAL JOURNAL OF NUMERICAL MODELLING: ELECTRONIC NETWORKS, DEVICES AND FIELDS
Int. J. Numer. Model. 2007; **20**:299–309
Published online 30 March 2007 in Wiley InterScience (www.interscience.wiley.com). DOI: 10.1002/jnm.647

A new approach for numerical simulation of quantum transport in double-gate SOI

Tarek M. Abdolkader*,†

Department of Basic Sciences, Benha Higher Institute of Technology, Egypt

SUMMARY

Numerical simulation of nanoscale double-gate SOI (Silicon-on-Insulator) greatly depends on the accurate representation of quantum mechanical effects. These effects include, mainly, the quantum confinement of carriers by gate-oxides in the direction normal to the interfaces, and the quantum transport of carriers along the channel. In a previous work, the use of transfer matrix method (TMM) was proposed for the simulation of the first effect. In this work, TMM is proposed to be used for the solution of Schrodinger equation with open boundary conditions to simulate the second quantum-mechanical effect. Transport properties such as transmission probability, carrier concentration, and *I–V* characteristics resulting from quantum transport simulation using TMM are compared with that using the traditional tight-binding model (TBM). Comparison showed that, when the same mesh size is used in both methods, TMM gives more accurate results than TBM. Copyright © 2007 John Wiley & Sons, Ltd.

Received 19 September 2006; Accepted 12 February 2007

KEY WORDS: double-gate devices; quantum transport; numerical simulation; transfer matrix method

1. INTRODUCTION

Continuing advances in integrated circuit technology results in a variety of new device structures with feature size in the nanometer range. With those advances, two main challenges arise: (1) the modelling of the complex physical phenomena that control the device behaviour in the so extremely small dimensions; and (2) the prediction of the response of novel device geometries. Technology computer aided design (TCAD) simulation tools are valuable aids to cope with both of the two challenges. For modelling physical phenomena, TCAD tools become indispensable as analytical models are no longer feasible. On the other hand, trend analysis

*Correspondence to: Tarek M. Abdolkader, Department of Basic Sciences, Benha Higher Institute of Technology, Egypt.
†E-mail: tarik_mak@hotmail.com, tarik_mak@gawab.com

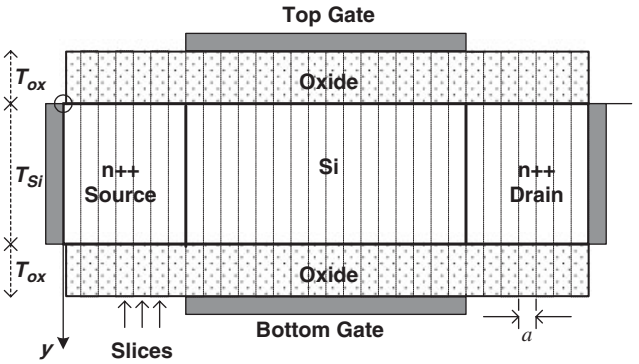

Figure 1. A model double-gate SOI device divided into vertical slices.

using TCAD tools have been successfully applied to optimize the device operation at a time when such transistors were not readily manufacturable [1].

Double-gate (DG) SOI transistors have emerged as promising devices for very large-scale integration circuits due to their better scalability compared to bulk CMOS [2]. The transport of carriers in the channel of a DG SOI (Figure 1) is controlled by two (top and bottom) gates. Numerical simulation of nanoscale DG SOI on the quantum level includes the solution of Poisson equation and Schrodinger equation self-consistently [3,4]. Usually, the numerical solution of Schrodinger equation in DG SOI is not implemented directly into two dimensions as this needs excessive computational burden; instead, it is solved by what is called mode-space representation [5]. In mode-space representation, Schrödinger equation is solved separately into two directions: the first direction is normal to the interface (transverse direction, y), in which, the carriers are confined by the upper and lower gate-oxides, and the second direction is parallel to the interface (longitudinal direction, x), in which, the domain of solution is bounded by two reservoirs of carriers (source and drain contacts). The first problem is 1D bounded problem which results in discrete energy levels (eigenvalues) and corresponding carrier distribution functions (eigenfunctions). The second problem is 1D unbounded problem, in which, the solution is found by the integration of the eigenfunctions of a continuum of energies. This integration is accomplished separately for carriers from both source and drain contacts and the overall solution is the sum of the two integrations.

In a previous work [6], transfer matrix method (TMM) [7,8] was proposed to be used to solve the first problem (bounded problem). In this work, TMM is proposed to be used for the simulation of quantum transport through solution of the Schrodinger equation with open boundary conditions (second problem). The transport is assumed ballistic [9], so no scattering effects are included. Transport properties of DG SOI such as transmission probability, carrier concentration, and I–V characteristics, resulting from simulation using TMM are compared with that using tight-binding model (TBM) [10] which is traditionally used for the discretization of Schrodinger equation.

In Section 2, the building blocks of device simulation on the quantum level are presented along with an explanation for how Schrodinger equation is solved using mode-space representation. The standard TBM approach used for quantum transport simulation is explained in Section 3 while new TMM approach is given in Section 4. A group of results that

DOI: 10.1002/jnm

evaluate the use of TMM compared to TBM are shown and discussed in Section 5. Finally, conclusion is given in Section 6.

2. QUANTUM SIMULATION OF DG SOI

Nanoscale DG MOSFET numerical simulation is performed by the self-consistent solution of Poisson equation and Schrodinger equation [3,4]. Poisson equation is given as

$$\nabla^2 V = -\frac{q}{\varepsilon}(p - n + N_{\mathrm{D}} - N_{\mathrm{A}}) \tag{1}$$

in which the electrical potential V can be determined given the quantities in the right-hand side including hole and electron distributions p and n, and doping concentrations for donors and acceptors N_{D} and N_{A}, respectively. In (1) q is electronic charge, and ε is the permittivity of the medium. On the other hand, Schrödinger equation with effective mass approximation can be written as

$$\frac{-\hbar^2}{2m^*}\nabla^2\psi - (qV + E)\psi = 0 \tag{2}$$

which, given the electric potential V, determines eigenenergies E and eigenfunctions ψ from which the carrier concentrations can be obtained. In (2), $\hbar$ is the modified Planck's constant and m^* is the effective mass of carriers. Equations (1) and (2) are coupled such that the solution of any one requires the result of the other; consequently, they are solved by iterative method until self-consistence is obtained.

The Schrödinger equation is discretized using mode-space representation approach which greatly reduces the size of the problem and provides sufficient accuracy when compared to full 2D spatial discretization [5]. Referring to Figure 1, a model DG SOI device is divided into vertical slices, each of width a. For each vertical slice at $x = x'$, a 1D effective mass equation in the y-direction is written as

$$\frac{-\hbar^2}{2m_y^*}\frac{\mathrm{d}^2\psi(x', y)}{\mathrm{d}y^2} + (U(x', y) - E)\psi(x', y) = 0 \tag{3}$$

where m_y^* is the effective mass of electrons in the y-direction and $U = -qV$ is the potential energy. Equation (3) represents a 1D-bounded problem whose solution details can be found in [6]. The solution results in a discrete set of eigenenergies and corresponding eigenfunctions, i.e. a set of modes. For each mode m, the distribution of eigenenergies $E_m(x)$ along the x-direction resulting from the solution of (3) is used to solve the 1D Schrödinger equation in the x-direction

$$\frac{-\hbar^2}{2m_x^*}\frac{\mathrm{d}^2\varphi^{(m)}(x)}{\mathrm{d}x^2} - (E - E_m(x))\varphi^{(m)}(x) = 0 \tag{4}$$

subject to open boundary conditions at source (left boundary) and drain (right boundary), where m_x^* is the effective mass of electrons in the x-direction. Equation (4) is solved twice, one assuming a plane wave is incident from the source contact, in which the solution is termed as, $\varphi_{\mathrm{S}}^{(m)}(x)$, and the other assuming a plane wave is incident from the drain contact, where the solution is termed $\varphi_{\mathrm{D}}^{(m)}(x)$. Once $\varphi_{\mathrm{S}}^{(m)}(x)$ and $\varphi_{\mathrm{D}}^{(m)}(x)$ are found, the device parameters such as, the transmission probability, carrier density, and drain current can be calculated as given in Section 5.

DOI: 10.1002/jnm

The method of solution of Equation (4) is our concern in this work, in which, TMM is used to solve it in place of TBM which was previously used. The details of TBM and TMM are given in the following two sections, respectively.

3. TIGHT-BINDING MODEL

The domain of solution of (4) is the silicon channel whose boundaries are semi-infinite contacts (source and drain). Figure 2 shows a sketch of the subband energy distribution along the channel, which plays the role of the potential function in (4). Since inside the boundary regions, the potential is uniform, plane wave solution is assumed there. The solution starts with assuming a wave of unit amplitude is injected from the source contact and results in a wave function $\varphi_{\mathrm{S}}^{(m)}(x)$. A portion of this wave is reflected to source in the negative x-direction and the other is transmitted to the drain in the positive x-direction. Consequently, the wave function values inside the boundaries can be written as [11]

$$\varphi_{\mathrm{S}}^{(m)}(x) = 1\mathrm{e}^{\mathrm{i}k_{\mathrm{S}}x} + r\mathrm{e}^{-\mathrm{i}k_{\mathrm{S}}x} \quad (x<0) \tag{5a}$$

$$\varphi_{\mathrm{S}}^{(m)}(x) = t\mathrm{e}^{\mathrm{i}k_{\mathrm{D}}x} \quad (x>L) \tag{5b}$$

where

$$k_{\mathrm{S,D}} = \sqrt{2m_x^*(E-U_{\mathrm{S,D}})}/\hbar \tag{6}$$

In TBM, the domain of solution is divided into small intervals of width a bounded by nodal points $1, 2, \ldots, N$. Equation (4) is then written at any nodal point i using finite-difference approximation [10] (the subscript S in $\varphi_{\mathrm{S}}^{(m)}(x)$ is omitted hereinafter for clarity)

$$-\eta(\varphi_{i-1}^{(m)} - 2\varphi_i^{(m)} + \varphi_{i+1}^{(m)}) + U_i\varphi_i^{(m)} = E\varphi_i^{(m)}$$

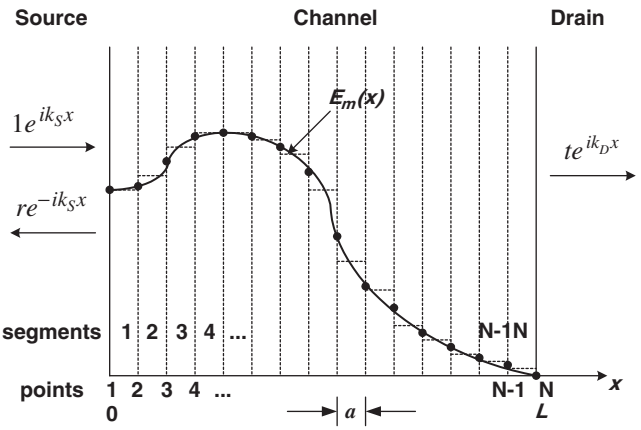

Figure 2. The domain of solution for Equation (4). The boundaries are two semi-infinite contacts (source and drain) at which plane waves are assumed. The wave function at the boundaries is shown here assuming a unit amplitude wave is incident from left.

DOI: 10.1002/jnm

or

$$-\eta\varphi_{i-1}^{(m)} + (2\eta + U_i - E)\varphi_i^{(m)} - \eta\varphi_{i+1}^{(m)} = 0, \quad i \leqslant i \leqslant N \tag{7}$$

where $\eta = \hbar^2/2m^*a^2$. The boundary conditions are incorporated in the equations of points 1 and N, at which (5a) and (5b) are used, respectively. On eliminating r and t, equations for nodal points 1 and N are given, respectively, as

$$(-\eta e^{ik_S a} + 2\eta + U_1 - E)\varphi_1^{(m)} - \eta\varphi_2^{(m)} = -2i\eta \sin(k_S a) \tag{8a}$$

$$-\eta\varphi_{N-1}^{(m)} + (2\eta + U_N - E - \eta e^{ik_D a})\varphi_N^{(m)} = 0 \tag{8b}$$

The system of equations (7) and (8) are solved for the wave function values $\varphi_S^{(m)}(x)$ at all nodal points. The parameters r and t can then be found from (5a) and (5b).

A similar argument can be traced assuming a wave is incident from the drain, which results in a wave function $\varphi_D^{(m)}(x)$. The boundary conditions are, in this case

$$\varphi_D^{(m)}(x) = 1e^{-ik_D x} + r'e^{ik_D x} \quad (x > L) \tag{9a}$$

$$\varphi_D^{(m)}(x) = t'e^{-ik_S x} \quad (x < 0) \tag{9b}$$

where k_S and k_D are the same as in (6). Finite-difference equations similar to (7) and (8) can be written and solved subject to the boundary conditions (9a) and (9b) to yield $\varphi_D^{(m)}(x)$, r', and t'. The solution of the whole system of equations is repeated at different values of energy that spans the whole $E^{(m)}(x)$ range.

4. TRANSFER MATRIX METHOD

In TMM, the channel is again divided into small segments of width a, and the potential within each segment is assumed constant as in TBM. However, in TMM, the wave function within any segment n is approximated as [8]

$$\varphi_n(x) = A_n \exp(\alpha_n x) + B_n \exp(-\alpha_n x) \tag{10}$$

where

$$\alpha_n = \sqrt{2m_x^*(U_n - E)}/\hbar \tag{11}$$

Applying the continuity conditions of $\varphi_n(x)$ and $d\varphi_n(x)/dx$ between each two successive segments, we arrive at a series of matrix equations relating A_n and B_n of any segment with those of the preceding segment A_{n-1} and B_{n-1} as follows:

$$\begin{bmatrix} A_{n-1} \\ B_{n-1} \end{bmatrix} = \mathbf{M}^{-1}(\alpha_{n-1}, x_{n-1})\mathbf{M}(\alpha_n, x_{n-1}) \begin{bmatrix} A_n \\ B_n \end{bmatrix} \tag{12}$$

where

$$\mathbf{M}(\alpha_n, x_m) = \begin{bmatrix} e^{\alpha_n x_m} & e^{-\alpha_n x_m} \\ \alpha_n e^{\alpha_n x_m} & -\alpha_n e^{-\alpha_n x_m} \end{bmatrix} \tag{13}$$

with $x_m = ma$, $m = 0, 1, 2, \ldots, N$.

DOI: 10.1002/jnm

Cascading all equations relating coefficients of successive segments to relate the coefficients of the left boundary to that of the right boundary [see (5)] yields

$$\begin{bmatrix} 1 \\ r \end{bmatrix} = \mathbf{W} \begin{bmatrix} t \\ 0 \end{bmatrix} \tag{14}$$

where

$$\mathbf{W} = \mathbf{M}^{-1}(\alpha_S, 0) \cdot \Pi \cdot \mathbf{M}(\alpha_D, L) \tag{15}$$

$$\mathbf{\Pi} = \mathbf{P}_1 \mathbf{P}_2 \ldots \mathbf{P}_N \tag{16}$$

$$\mathbf{P}_n = \mathbf{M}(\alpha_n, x_{n-1}) \mathbf{M}^{-1}(\alpha_n, x_n) \tag{17}$$

According to (14), r and t can be found in terms of the matrix elements of $\mathbf{W}$ defined in (15) as follows:

$$r = \mathbf{W}(2,1)/\mathbf{W}(1,1) \quad \text{and} \quad t = 1/\mathbf{W}(1,1) \tag{18}$$

Once r and t are known, all the coefficients A_n and B_n, and thus the wave function $\varphi_S^{(m)}(x)$, can be found from (12).

A similar procedure is followed assuming that the wave is incident from the drain rather than from the source. Using the boundary conditions given in (9), the equation relating left and right boundaries analogous to (14) will be

$$\begin{bmatrix} 0 \\ t' \end{bmatrix} = \mathbf{W} \begin{bmatrix} r' \\ 1 \end{bmatrix} \tag{19}$$

in which $\mathbf{W}$ has the same definition as (15)–(17). From (19), the unknown coefficients r' and t' are given as

$$\begin{aligned} r' &= -\mathbf{W}(1,2)/\mathbf{W}(1,1) \\ t' &= \mathbf{W}(2,2) - \mathbf{W}(1,2)\mathbf{W}(2,1)/\mathbf{W}(1,1) \end{aligned} \tag{20}$$

The wave function resulting from this solution is $\varphi_D^{(m)}(x)$. The solution for $\varphi_S^{(m)}(x)$ and $\varphi_D^{(m)}(x)$ is again repeated at different energies in the range of $E^{(m)}(x)$.

5. RESULTS AND DISCUSSION

The transport properties of a model DG SOI nMOSFET device were calculated using both TBM and TMM methods. These properties include the transmission probability of carriers through the channel, carrier density, and the drain current. For the comparison of accuracy of the two methods, the results obtained by either method at a very fine mesh (at a large number of segments) are taken as a reference. In this section, the methods of the calculation of the above-mentioned transport properties are first explained, then, the results for TBM and TMM are shown and discussed.

The transmission probability through the channel at a certain energy E, $\tau(E)$, can be found either from the parameter t given in (5b) or the parameter t' given in (9b) as follows [12]:

$$\tau(E) = |t|^2 k_D/k_S = |t'|^2 k_S/k_D \tag{21}$$

where k_S and k_D are given by (6).

DOI: 10.1002/jnm

On the other hand, the m-mode contribution to the total electron density is thus found from [11]

$$n^{(m)} = \frac{1}{\hbar a}\sqrt{\frac{m_y^* k_B T}{2\pi^3}} \times \int_0^\infty \Im_{-1/2}(F_S - E)|\varphi_S^{(m)}(x)|^2 + \Im_{-1/2}(F_D - E)|\varphi_D^{(m)}(x)|^2 \, dE \tag{22}$$

where m_y^* is the effective mass of electrons in the y-direction, k_B is the Boltzmann constant, T is the temperature, $\Im_{-1/2}$ is the Fermi–Dirac integral of order $-1/2$ [13], F_S and F_D are the Fermi levels at source and drain contacts, respectively. The total electron density within the device is found by the sum of all contributions of individual modes weighted by the probability function $|\psi_m(x, y)|^2$ of each mode resulting from the solution of (3), i.e.

$$n(x, y) = \sum_m n^{(m)} |\psi_m(x, y)|^2 \tag{23}$$

The electron current per unit energy per unit device width, transmitted from source to drain can be found at an energy E by [14]

$$I_D(E) = \frac{q}{\hbar^2}\sqrt{\frac{m_y^* k_B T}{2\pi^3}} \times [\Im_{-1/2}(F_S - E) - \Im_{-1/2}(F_D - E)]\tau(E) \tag{24}$$

The terminal drain current can be calculated by the integration of $I_D(E)$ over energy, i.e.

$$I_D = \int I_D(E) \, dE \tag{25}$$

The model device is chosen by the thickness of top and bottom oxides $T_{ox} = 1.6\,\text{nm}$ while that of the silicon film $T_{Si} = 3.2\,\text{nm}$. The source/drain donor doping is $10^{20}\,\text{cm}^{-3}$ and substrate body acceptor doping is $10^{10}\,\text{cm}^{-3}$. The top and bottom insulator relative dielectric constant is assumed to be 3.9, while that of Si is 11.7. The length of the channel is 12 nm and the length of source/drain region is 6 nm, thus the total length of the device is 24 nm. All simulations are performed at room temperature ($T = 300\,\text{K}$). It was found that a mesh of more than 120 segments corresponding to a mesh spacing less than 0.2 nm is adequately fine to make the results of the two methods indistinguishable. Consequently, this mesh size is used for extracting reference results.

Figure 3 shows the transmission probability as a function of energy when the model device is biased at a drain voltage $V_D = 0.1\,\text{V}$ and gate voltage (both gates) $V_G = 0.1\,\text{V}$. The figure shows the results of TBM (dotted line) and TMM (dashed line) using a mesh of spacing 1.6 nm (15 segments) for each. Reference results are also shown (solid line). It is evident from the figure that TMM results are more accurate than TBM results. This is ascertained in Figure 4, in which the errors in the calculation of the transmission probability using both methods relative to the reference values are depicted. To compare the accuracy at different mesh sizes, the maximum error in the calculation of the transmission probability by either method is drawn *versus* mesh spacing, a, as illustrated in Figure 5. At $a = 1.6\,\text{nm}$, TMM has an error that is 4.6 times less than TBM. It should be noted that for a prescribed error maximum of 0.05, mesh spacing used by TBM must not exceed 1.1 nm, while a mesh spacing of 1.6 nm is adequate when TMM is used.

For the assessment of accuracy in the calculation of carrier concentration, the 2D subband carrier density, N_sub, along the channel was simulated using both TBM and TMM with mesh

DOI: 10.1002/jnm

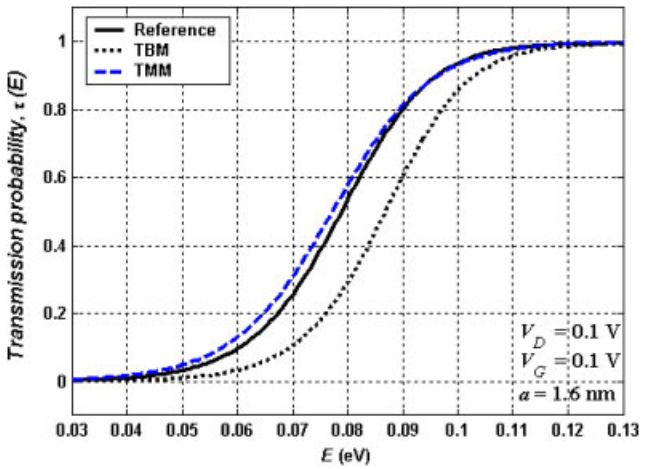

Figure 3. The distribution of transmission probability with energy in the DG-SOI model device calculated by either TBM (dotted line) or TMM (dashed line). The reference results calculated by a very fine mesh are also shown (solid line).

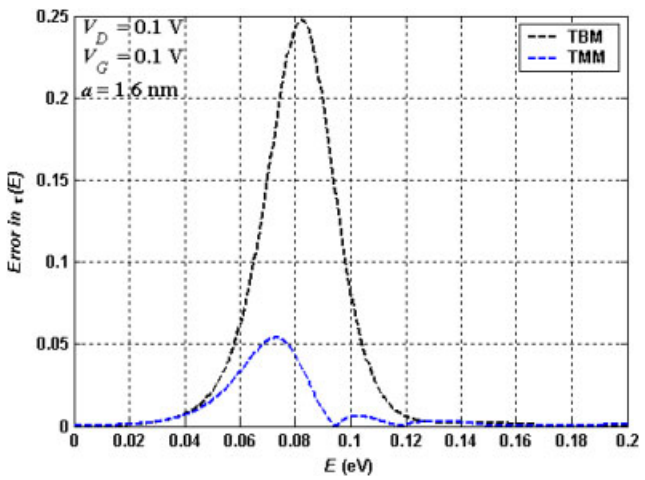

Figure 4. The error in the calculation of the transmission probability for the model DG-SOI device calculated by either TBM (dotted line) or TMM (dash-dotted line) both with mesh spacing $a = 1.6$ nm.

spacing 1.6 nm for each. The results are depicted in Figure 6 along with the reference curve calculated with TBM using mesh spacing 0.2 nm. Near the middle of the channel, TMM has more ability to follow the rapid variation of electron density than TBM.

The end objective of device simulation is to obtain the I_D–V_G characteristics of the device. Figure 7 illustrates the I_D–V_G characteristics of the chosen model DG SOI device extracted by TBM and TMM methods with the same mesh spacing $a = 1.6$ nm. Compared to the reference

DOI: 10.1002/jnm

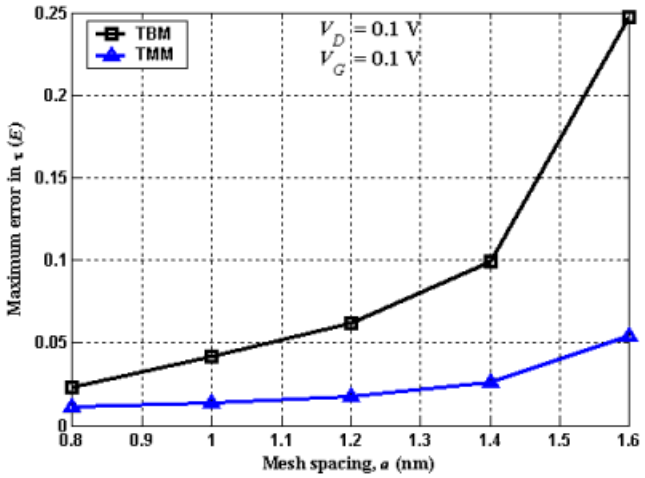

Figure 5. The maximum error in the transmission probability calculated by both TBM and TMM methods *versus* the mesh spacing a. At $a = 1.6$ nm, the maximum error of TMM is 4.6 times less.

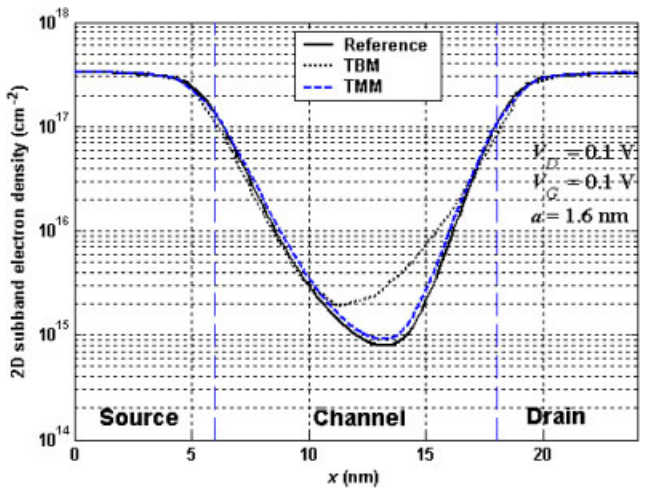

Figure 6. The 2D subband electron density along the channel of a model DG device. Results of TBM and TMM are compared to reference results.

I_D–V_G characteristics, TMM is more accurate. The error in the drain current ΔI_D of the two methods relative to the reference value is shown in Figure 8. At large gate bias voltages, TMM is nearly 90 μA/μm less in error than TBM, which illustrates the superiority of TMM over TBM.

DOI: 10.1002/jnm

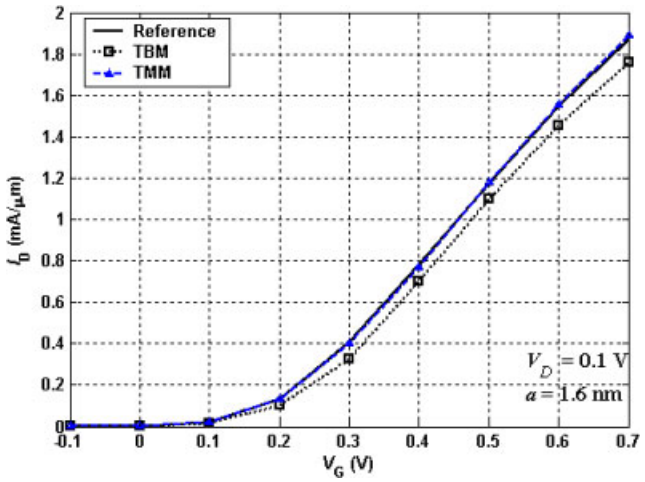

Figure 7. I_D–V_G characteristics of the model DG-SOI device simulated by TMM and TBM methods both with a mesh spacing of 1.6 nm. Reference results are also shown.

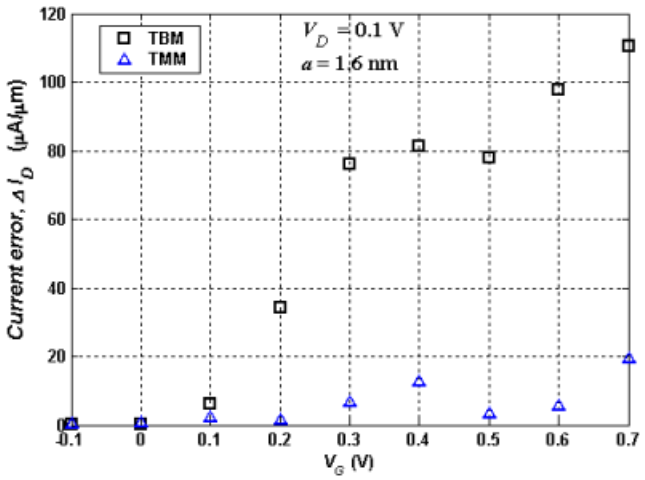

Figure 8. The relative error in the drain current of both TBM and TMM methods for the device with settings are given in Figure 7.

6. CONCLUSION

Transfer Matrix Method (TMM) was successfully used for the simulation of quantum transport in DG SOI MOSFETs. Transport properties of the device such as transmission probability at different energies, the 2D subband carrier density along the channel of the device, and I_D–V_G characteristics were simulated. All simulation results of TMM were compared with the

DOI: 10.1002/jnm

traditional tight-binding model (TBM) using the results at a very fine mesh as a reference. The comparison verified the superiority of TMM over TBM method for quantum transport simulation.

REFERENCES

1. Kenrow JA. Characterization and analysis of OFET devices based on TCAD simulations. *IEEE Transactions on Electron Devices* 2005; **52**(9):2034–2041.
2. Roy K, Mahmoodi H, Mukhopadhyay S, Ananthan H, Bansal A, Cakici T. Double-gate SOI devices for low-power and high-performance applications. *Proceedings of the 19th International Conference on VLSI Design* (*VLSID'06*), Hyderabad, India, 3–7 January 2006; 445–452.
3. Abdolkader TM. Modeling and 2D simulation of double-gate SOI devices. *Ph.D. Dissertation*, Faculty of Engineering, Ain-Shams University, Cairo, Egypt, 2005.
4. Abdolkader TM, Fikry W, Omar OA, Fathi M. FETMOSS: a software tool for 2D simulation of double-gate MOSFETs. *International Journal of Numerical Modeling*: *Electronic Networks*, *Devices*, *and Fields* 2006; **19**:301–314.
5. Venugopal R, Ren Z, Datta S, Lundstrom MS. Simulating quantum transport in nanoscale MOSFETs: real versus mode space approaches. *Journal of Applied Physics* 2002; **92**:3730–3739.
6. Abdolkader TM, Hassan HH, Fikry W, Omar OA. Solution of Schrödinger equation in double-gate MOSFETs using transfer matrix method. *Electronic Letters* 2004; **40**(20):1307–1308.
7. Gilfoyle GP. A new teaching approach to quantum mechanical tunneling. *Mathematica in Education and Research* 1995; **4**(1):19–23.
8. Kalotas TM, Lee AR. A new approach to one-dimensional scattering. *American Journal of Physics* 1991; **59**:48–52.
9. Lundstrom M. Elementary scattering theory of the MOSFET. *IEEE Electron Device Letters* 1997; **18**:361–363.
10. Datta S. *Electronic Transport in Mesoscopic Systems* (sec. 3.5). Cambridge University Press: Cambridge, U.K., 2002.
11. Ren Z, Venugopal R, Goasguen S, Datta S, Lundstrom MS. nanoMOS 2.5: a two-dimensional simulator for quantum transport in double-gate MOSFETs. *IEEE Transactions on Electron Devices* 2003; **50**:1914–1925.
12. Ferry DK. *Quantum Mechanics An Introduction to Device Physicists and Electrical Engineers* (2nd edn, sec. 3.2). IOP Publishing Ltd: London, 2001.
13. Blakemore JS. Approximation of Fermi–Dirac integrals especially the functions $F_{1/2}(\eta)$ to describe electron density in a semiconductor. *Solid State Electronics* 1982; **25**:1067.
14. Ren Z. Nanoscale MOSFETs: physics, simulation, and design. *Ph.D. Dissertation*, Purdue University, West Lafatette, IN, 2001.

AUTHOR BIOGRAPHY

Tarek M. Abdolkader was born in Cairo, Egypt in 1970. He received BS degree in Electrical Engineering (Electronics and Communications) from the faculty of Engineering, Ain-Shams university, Cairo in 1992, another BS degree in physics from the faculty of Science, Ain-Shams university, Cairo in 1996, MS and PhD degrees in Engineering physics from the faculty of Engineering, Ain-Shams university, Cairo in 2001 and 2005, respectively. He is currently an assistant professor of Engineering physics at the department of basic sciences, Benha Higher institute of Technology, Benha, Egypt. His research interests are modeling of quantum-mechanical effects and development of simulation tools for modern electronic devices, especially, double-gate SOI MOSFETs.

DOI: 10.1002/jnm